Molecular Biology of the Cell
Vol. 19, 2682–2695, July 2008

UNC-108/Rab2 Regulates Postendocytic Trafficking in *Caenorhabditis elegans*

Denise K. Chun,* Jason M. McEwen,*† Michelle Burbea, and Joshua M. Kaplan

Department of Molecular Biology, Massachusetts General Hospital, and Department of Genetics, Harvard Medical School, Boston MA 02114

Submitted November 8, 2007; Revised April 8, 2008; Accepted April 11, 2008
Monitoring Editor: Sandra Lemmon

After endocytosis, membrane proteins are often sorted between two alternative pathways: a recycling pathway and a degradation pathway. Relatively little is known about how trafficking through these alternative pathways is differentially regulated. Here, we identify UNC-108/Rab2 as a regulator of postendocytic trafficking in both neurons and coelomocytes. Mutations in the *Caenorhabditis elegans* Rab2 gene *unc-108*, caused the green fluorescent protein (GFP)-tagged glutamate receptor GLR-1 (GLR-1::GFP) to accumulate in the ventral cord and in neuronal cell bodies. In neuronal cell bodies of *unc-108*/Rab2 mutants, GLR-1::GFP was found in tubulovesicular structures that colocalized with markers for early and recycling endosomes, including Syntaxin-13 and Rab8. GFP-tagged Syntaxin-13 also accumulated in the ventral cord of *unc-108*/Rab2 mutants. UNC-108/Rab2 was not required for ubiquitin-mediated sorting of GLR-1::GFP into the multivesicular body (MVB) degradation pathway. Mutations disrupting the MVB pathway and *unc-108*/Rab2 mutations had additive effects on GLR-1::GFP levels in the ventral cord. In coelomocytes, postendocytic trafficking of the marker Texas Red-bovine serum albumin was delayed. These results demonstrate that UNC-108/Rab2 regulates postendocytic trafficking, most likely at the level of early or recycling endosomes, and that UNC-108/Rab2 and the MVB pathway define alternative postendocytic trafficking mechanisms that operate in parallel. These results define a new function for Rab2 in protein trafficking.

INTRODUCTION

Fast excitatory transmission in the mammalian CNS is mediated primarily by two families of glutamate receptors (GluRs): α-amino-3-hydroxy-5-methyl-4-isoxazolepropionic acid (AMPA) receptors and *N*-methyl-D-aspartate (NMDA) receptors. Work from several laboratories suggests that regulation of the abundance of AMPA receptors is a cellular mechanism for producing activity-dependent changes in synaptic strength, e.g., long-term potentiation (LTP), long-term depression, and homeostatic plasticity (Malinow and Malenka, 2002; Song and Huganir, 2002; Bredt and Nicoll, 2003; Park *et al*., 2004). For these reasons, there is great interest in defining the mechanisms that regulate the trafficking of AMPA receptors.

AMPA receptors at synapses are derived from a recycling pool of receptors (Ehlers, 2000; Lin *et al*., 2000). The rate of AMPA receptor exocytosis and endocytosis is regulated by synaptic activity (Ehlers, 2000). After endocytosis, AMPA receptors are sorted into either of two postendocytic pathways: the recycling endosome (from which receptors are recycled to the plasma membrane) or late endosomes/lysosomes (where receptors are degraded) (Ehlers, 2000; Lee *et al*., 2004). Recycling endosomes are thought to be the source of AMPA receptors involved in activity-dependent potentiation of synapses (Park *et al*., 2004). Although substantial progress has been made in understanding the endocytosis of AMPA receptors, much remains to be learned about the mechanisms by which AMPA receptors are sorted between these two postendocytic pathways.

Rab GTPases are thought to play a pivotal role in orchestrating the specificity of membrane trafficking events (Chavrier and Goud, 1999; Zerial and McBride, 2001; Grosshans *et al*., 2006). Rabs comprise the largest class of Ras-like GTPases, and they have been implicated in many aspects of intracellular membrane trafficking, such as vesicle budding from donor compartments, and vesicle tethering and fusion with target membranes. Each Rab seems to function in specific membrane transport steps, and this specificity arises from the selective recruitment and activation of Rabs on specific membranes. Association and dissociation of Rabs with their cognate membranes is coupled to the hydrolysis of their bound guanine nucleotides. Thus, nucleotide hydrolysis is required for Rabs to perform their membrane transport functions (Grosshans *et al*., 2006).

The nematode *Caenorhabditis elegans* has been used as a genetic model to study the trafficking of an AMPA-type glutamate receptor GLR-1. GLR-1 is expressed in ventral cord interneurons (Hart *et al*., 1995; Maricq *et al*., 1995), where it is localized to sensory–interneuron and interneuron–interneuron synapses (Rongo and Kaplan, 1999; Burbea *et al*., 2002). We previously showed that the synaptic abundance of GLR-1 receptors is regulated by clathrin-mediated endocytosis and by ubiquitin ligases (Burbea *et al*., 2002; Juo and Kaplan, 2004; Dreier *et al*., 2005), as are mammalian AMPA receptors (Carroll *et al*., 1999; Man *et al*., 2000; Colledge *et al*., 2003; Patrick *et al*., 2003). In previous studies,

This article was published online ahead of print in *MBC in Press* (http://www.molbiolcell.org/cgi/doi/10.1091/mbc.E07–11–1120) on April 23, 2008.

* These authors contributed equally to this work.

† Present address: Department of Biological Chemistry, University of California Los Angeles, Los Angeles, CA 90095.

Address correspondence to: Joshua M. Kaplan (kaplan@molbio.mgh.harvard.edu).

mammalian Rab2 has been proposed to regulate retrograde trafficking between pre-Golgi intermediate compartment (ERGIC) and the endoplasmic reticulum (ER) (Tisdale and Balch, 1996; Tisdale and Jackson, 1998). Here, we show that UNC-108/Rab2 plays a role in postendocytic trafficking of GLR-1 and other cargo in neurons. We also show that UNC-108/Rab2 is necessary for proper trafficking of postendocytic cargo in coelomocytes. Thus, our results identify a new function for Rab2.

MATERIALS AND METHODS

Strains

Strains were maintained as described by Brenner at 20°C (Brenner, 1974). The following strains were used in this study: N2 Bristol, *unc-108(nu415)*, *unc-67(e713)*, *unc-108(n501)*, *unc-108(n777)*, *nuIs24* (P*glr-1*::GLR-1::GFP), *bIs33* (P*rme-8*::RME-8::GFP), *nuEx1324* (P*snb-1*::UNC-108::FLAG), *nuEx1325* (P*glr-1*::UNC-108::FLAG), *nuEx1326* (P*unc-17*::UNC-108::FLAG), *nuEx1327* (P*myo-3*::UNC-108::FLAG), *nuIs125* (P*glr-1*::GFP::SNB-1), *nuEx1328* (ssVenus::KDEL), *nuEx1328* (ssVenus::AAAA), *nuEx1329* (P*glr-1*::ssTomato::KDEL), *nuEx1330* (P*glr-1*::RFP::BET-1), *nuEx1331* (P*glr-1*::RFP::GOS-28), *nuEx1332* (P*glr-1*::RFP::Syntaxin-16), *nuEx1333* (P*glr-1*::Cherry::Rab10), *nuEx1334* (P*glr-1*::Cherry::Rab8), *nuEx1335* (P*glr-1*::Cherry::Rab14), *nuEx1336* (P*glr-1*::Cherry::Rab11), *nuEx1337* (P*glr-1*::RFP::Syntaxin-13), *nuEx1338* (P*glr-1*::Cherry::Rab5), *nuEx1339* (P*glr-1*::Cherry::Rab7), *nuIs232* (P*glr-1*::GFP::Syntaxin-13), *nuEx1340* (P*glr-1*::RFP::Syntaxin-5), *nuEx1341* (P*unc-122*::UNC-108::FLAG), *nuIs145* (*vps-4(DN)*), *nuIs89* (P*glr-1*::MUb) *nuEx1345* (P*glr-1*::GFP::BET-1) *nuEx1351* (P*unc-129*::GFP::UNC-64, P*unc-129*::RFP::KDEL), *nuEx1350* (P*glr-1*::UNC-108::FLAG, P*glr-1*::RFP::BET-1), and *nuEx1352* (P*glr-1*::UNC-108 (Q65L)::FLAG).

Cloning of unc-108(nu415)

The *unc-108(nu415)* allele was mapped based on the Uncoordinated (Unc) phenotype after back crosses revealed close linkage to the GLR-1::GFP phenotype. *unc-108(nu415)* was initially isolated using the *nuIs25* (P*glr-1*::GLR-1::GFP) strain, and it was linked to the *nuIs25* transgene demonstrating that *nu415* is on chromosome I. Five Unc genes located on chromosome I were tested for complementation based on similar Unc phenotypes: *unc-40*, *unc-14*, *unc-67*, *unc-87*, and *unc-59*. *unc-108(nu415)* and *unc-67(e713)* failed to complement, indicating that they are allelic. *unc67(e713)* was a previously uncloned Unc gene.

Mapping of *nu415*, was performed by crossing into CB4856 Hawaiian worms and using polymorphism-based Snip-single-nucleotide polymorphism (SNP) mapping (Wicks *et al*., 2001). *unc-108(nu415)* was positioned between two SNPs at positions −3.16 and −1.65 on chromosome I. This region of 1.51 map units was spanned by 14 cosmids. Cosmid injections identified that cosmid F53F10 was sufficient to rescue the Unc phenotype. Fragments of this cosmid were injected in order to test for single gene rescue and a BamHI/Eag I (4.7-kb) fragment of F53F10 that contained only the *unc-108* genomic region was able to rescue the Unc phenotype.

Constructs and Transgenes

The *unc-108* rescuing promoter consisted of 2.3 kb upstream of the *unc-108* start codon. This promoter fragment was amplified to add SphI and BamHI sites and cloned into the Fire lab vector pPD 95.75 to place it upstream of soluble GFP. *unc-108* cDNA was isolated from wild-type worms and cloned into the Fire vector pPD 49.26 with either the *glr-1* or the *unc-108* promoter. To observe UNC-108 localization, GFP was added to the N terminus of UNC-108, but this construct was unable to rescue the *unc-108(nu415)* Unc or the GLR-1::GFP phenotype. Therefore, a rescuing construct was made by inserting a FLAG epitope after amino acid 191 (at the end of homology with mammalian Rab2). The UNC-108::FLAG construct was cloned into pPD 49.26 and the following promoters were then inserted: P*unc-108*, P*snb-1*, P*glr-1*, P*unc-17*, and P*myo-3*. UNC-108 with the point mutation Q65L contains a FLAG epitope at amino acid 191 and was placed under the P*glr-1* promoter.

Subcellular markers consisting of either soluble *N*-ethylmaleimide-sensitive factor attachment protein receptor SNARE proteins or Rab proteins were generated by insertion of a NotI restriction site immediately following the start codon ATG and insertion of a NotI-flanked RFP (mCherry) or GFP. ssVenus::KDEL and ssVenus::AAAA were generated by fusing the Pat-3 signal sequence upstream of the Venus (yellow fluorescent protein [YFP] variant) and adding the sequence encoding either the KDEL signal or four Alanines before the Venus stop codon. ssTomato::KDEL was generated by creating a sequence that consisted of the Pat-3 signal sequence a NotI restriction site encoding three alanines (GCGGCCGCC) followed by the KDEL sequence, and a NotI-flanked Tomato was then cloned in. These markers were then cloned into pPD 49.26 containing the *glr-1* promoter. Dominant-negative VPS-4 (*vps-4(DN)*) was generated by making a single amino acid change from K164 to Q. *vps-4* (K164Q) was coned into pPD 49.26 containing the *glr-1* promoter. Injection of all constructs into worms was performed as described previously to generate transgenic lines. Both *vps-4(DN)* and GFP::Syntaxin-13 were integrated into chromosomes using a UV cross-linker (Fisher Science, Pittsburgh, PA). The RME-8::GFP strain was a gift from Barth Grant (Rutgers University, Piscataway, NJ).

Immunolabeling, Endoglycosidase H (Endo H) and peptide-N^{-}-(N-acetyl-β-glucosaminyl)asparagine Amidase (PNGase F) Treatment, and Western Blot Analysis

For immunolabeling experiments, *nuEx1324* and *nuEx1350* worms were fixed using Bouin's fixative and labeled with antibodies to the FLAG epitope (M2 antibody; Sigma-Aldrich, St. Louis, MO) and red fluorescent protein (RFP) (DsRed polyclonal antibody; Clontech, Palo Alto, CA) at a concentration of 1:500, and subsequently, Alexa Fluor 488-conjugated and Alexa Fluor 594-conjugated secondary antibodies (Invitrogen, Carlsbad, CA) were then applied at a concentration of 1:500. Animals were mounted on slides and imaged. Endogenous UNC-108 protein was visualized on Western blot by boiling wild-type and *unc-108(nu415)* worms in 5× SDS sample buffer and loading the lysates onto an SDS denaturing gel. Western blots were performed using an antibody against full-length mouse Rab2 (Santa Cruz Biotechnology, Santa Cruz, CA). UNC-108::FLAG protein was analyzed in extracts prepared from *nuEx1323* (P*unc-108*::UNC-108::FLAG) worms by immunoblotting with an anti-FLAG antibody (Sigma-Aldrich).

For Endo H and PNGase F assays, lysates were made by boiling worms in 5× denaturing buffer (2.5% SDS and 5% beta-mercaptoethanol) followed by sonication. Lysates were then diluted to 1× denaturing buffer in water plus protease inhibitors (10 μg/ml leupeptin, 5 μg/ml chymostatin, 3 μg/ml elastinal, 1 μg/ml pepstatin A, and 1 mM phenylmethylsulfonyl fluoride). Digests were then performed as recommended by the enzyme manufacturer (New England Biolabs, Ispwich, MA). Treated and untreated lysates were run on SDS denaturing gels. Western blots were performed on samples using an anti-GFP antibody (JL-8; Clontech). GLR-1::GFP levels were measured by boiling a mixed population of worms in 5X SDS sample buffer and loading on a SDS denaturing gel. Blots were then probed with a GFP antibody (JL-8; Clontech). Samples were normalized for protein levels by measuring actin levels by using an anti-actin antibody (MP Biomedicals, Irvine, CA). For Endo H and protein level measurements, five independent populations were measured for each genotype. Quantitative imaging of Western blots was performed using a Typhoon Trio Plus variable mode imager and ImageQuant TL version 2005 software (GE Healthcare, Chalfont St. Giles, United Kingdom).

Imaging

Fluorescent imaging of the ventral nerve cord was performed using an Axiovert 100 microscope (Carl Zeiss, Jena, Germany) and PlanApo 100× (1.4 numerical aperture [NA]) (Olympus, Tokyo, Japan) objective equipped with fluorescein isothiocyanate/GFP or RFP filters and an ORCA100 charge-coupled device camera (Hamamatsu, Bridgewater, NJ). Antibody stained animals were mounted on agarose pads and imaged. Live animals were immobilized with 30 mg/ml butanedione monoxime (BDM; Sigma-Aldrich). Image stacks were captured and maximum intensity projections were obtained using MetaMorph 4.5 software (Molecular Devices, Sunnyvale, CA). Identical camera gain, exposure settings, and fluorescence filters were used for all live animal imaging.

Line scans of ventral nerve cord fluorescence were analyzed in IGOR Pro (WaveMetrics, Portland, OR) using custom-written software (Burbea *et al*., 2002; Sieburth *et al*., 2005). Arc lamp output was normalized by measuring fluorescence of 0.5 μm FluoSphere beads (Invitrogen) for each day. Fluorescence amplitude for puncta peak and cord values was normalized to wild-type controls to facilitate comparison. Statistical significance was calculated using a Student's *t* test as described previously.

Fluorescent imaging of neuronal cell bodies and coelomocytes was performed on an Olympus Fluoview FV1000 confocal laser scanning microscope by using a Olympus PlanApo N 60× objective (1.45 NA). Animals imaged for neuronal cell bodies were immobilized with 30 mg/ml BDM (Sigma-Aldrich). Coelomocyte images were captured after injection of Texas Red-bovine serum albumin (TR-BSA) as described previously (Zhang *et al*., 2001): animals were put on ice for 10 min to arrest endocytosis then fixed in 1% paraformaldehyde for 10 min before imaging. For both neuronal cell bodies and coelomocytes, Z-stacks were taken of the entire cell, and a representative single plane was selected.

For quantification of GLR-1::GFP colocalization with RFP-tagged compartment markers in *unc-108(nu415)* mutant neuronal cell bodies, a region of interest was drawn around a GLR-1::GFP tubulovesicular structure, and this image was thresholded so that all pixels below 1 SD of the mean pixel intensity calculated for the region of interest were excluded. The percent area colocalization of the thresholded GLR-1::GFP images and the various RFP-tagged compartment markers were then measured (using MetaMorph software), and statistical significance was calculated using a Student's *t* test as described previously. To compare quantitatively the colocalization of GLR-1::GFP with a particular RFP-tagged marker in wild type versus *unc-108* mutant neuronal cell bodies, a slightly different strategy for thresholding was used. The pixel intensity corresponding to the cut-off for the brightest 5% of pixels in individual images of GLR-1::GFP in both wild-type and *unc-*

108(nu415) neuronal cell bodies was calculated by plotting the cumulative percentage of total pixel count against pixel intensity. The pixel intensity corresponding to the brightest 5% of pixels in the GLR-1::GFP image was then used as the threshold for the image, and these thresholded GLR-1::GFP images were subsequently used to determine the percent area colocalization with their respective RFP-tagged compartment markers.

RESULTS

Gain- and Loss-of-Function unc-108/Rab2 Alleles Cause Similar Locomotion Defects

We isolated the *nu415* allele as a mutation that altered the localization of GLR-1::GFP in the ventral nerve cord (detailed below). We positionally cloned *nu415*, finding that it corresponds to a deletion in the *unc-108* gene, which encodes the *C. elegans* orthologue of Rab2 (Figure 1A). The *nu415* mutation deletes the codons encoding the carboxy-terminal 66 amino acids, including the putative geranylation site. An anti-mouse Rab2 antibody detected a 23-kDa protein in extracts prepared from wild-type controls, and this band was absent in homozygous *unc-108(nu415)* mutants (Figure 1B). These results suggest that the *nu415* mutation produces a severe loss of *unc-108*/Rab2 function.

Homozygous *unc-108(nu415)* mutants had an uncoordinated locomotion phenotype (Figure 1C), which had a recessive pattern of inheritance (data not shown). A second genetic locus in this region, *unc-67*, was defined by a single allele (*e713*) that causes a similar recessive uncoordinated phenotype. We found that *e713* corresponds to a G184E missense mutation in *unc-108*. In addition, *e713* failed to complement *nu415* for the locomotion defect (data not shown). The G184 residue is conserved in other Rab GTPases (Rab4 and Rab14), and it is located within the Rab hypervariable domain, which is important for guanine nucleotide dissociation inhibitor and geranylgeranyl trans-

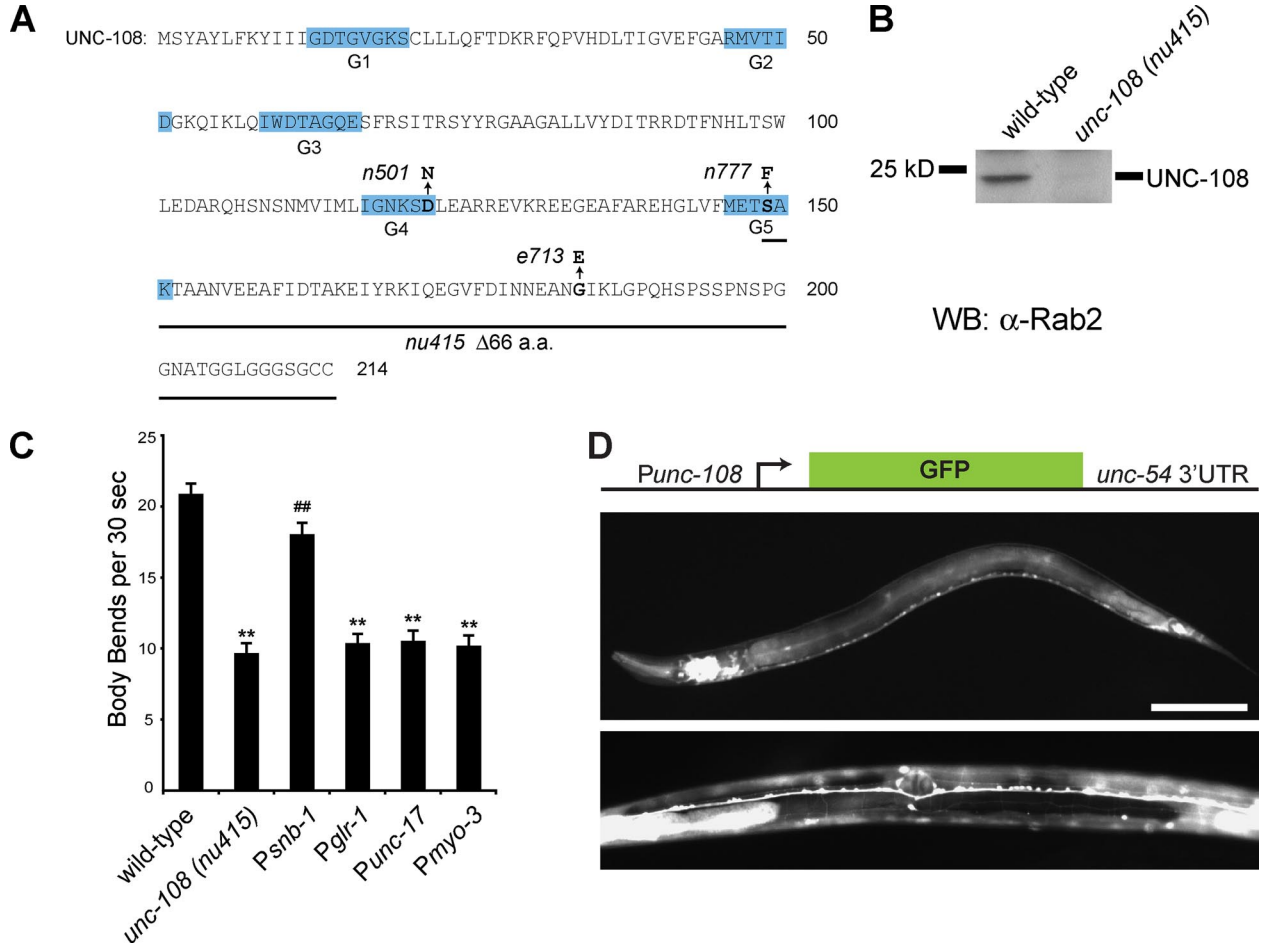

Figure 1. UNC-108/Rab2 functions in the nervous system of *C. elegans*. (A) The amino acid sequence of the UNC-108 protein is shown. Alleles are marked with arrows pointing to the amino acid transition for each missense mutation. The conserved G1–G5 motifs involved in GTP binding are highlighted in blue. The solid line below the sequence represents the 66-amino acid deletion in the *nu415* allele. (B) An anti-mouse RAB2 antibody (Santa Cruz Biotechnology) detects UNC-108 as a 23-kDa band on a Western blot of extracts prepared from wild-type worms but not from *unc-108(nu415)* mutants. (C) The number of body bends per 30 s was counted for wild-type, *unc-108(nu415)*, and *unc-108(nu415)* animals expressing FLAG-tagged UNC-108 under the following promoters: *snb-1* (pan-neuronal Synaptobrevin), *glr-1*, *unc-17* (cholinergic motorneurons), and *myo-3* (body wall muscle) (n = 20 for each). *unc-108(nu415)* animals show a 54% decrease in body bends as compared with wild-type control worms ($p < 0.0001$). Expression of FLAG-tagged UNC-108 under the *glr-1*, *unc-17*, and *myo-3* promoters did not rescue the locomotion defect in *unc-108(nu415)* mutants. Expression of FLAG-tagged UNC-108 under the *snb-1* promoter restored locomotion to 86% of that of wild type ($p = 0.014$ compared with wild-type, $p < 0.0001$ compared with *nu415*) in *unc-108(nu415)* mutant worms. (D) A 2.5-kb promoter fragment of the *unc-108* gene was cloned upstream of GFP followed by the *unc-54* 3′ UTR. Stage three larval (L3) worms expressing this transcriptional reporter construct were imaged. Bar, 50 μm. Error bars indicate SEM. **$p < 0.001$, statistical significance of compared with wild type; ##$p < 0.001$ indicates statistical significance compared with *unc-108(nu415)* (Student's *t* test).

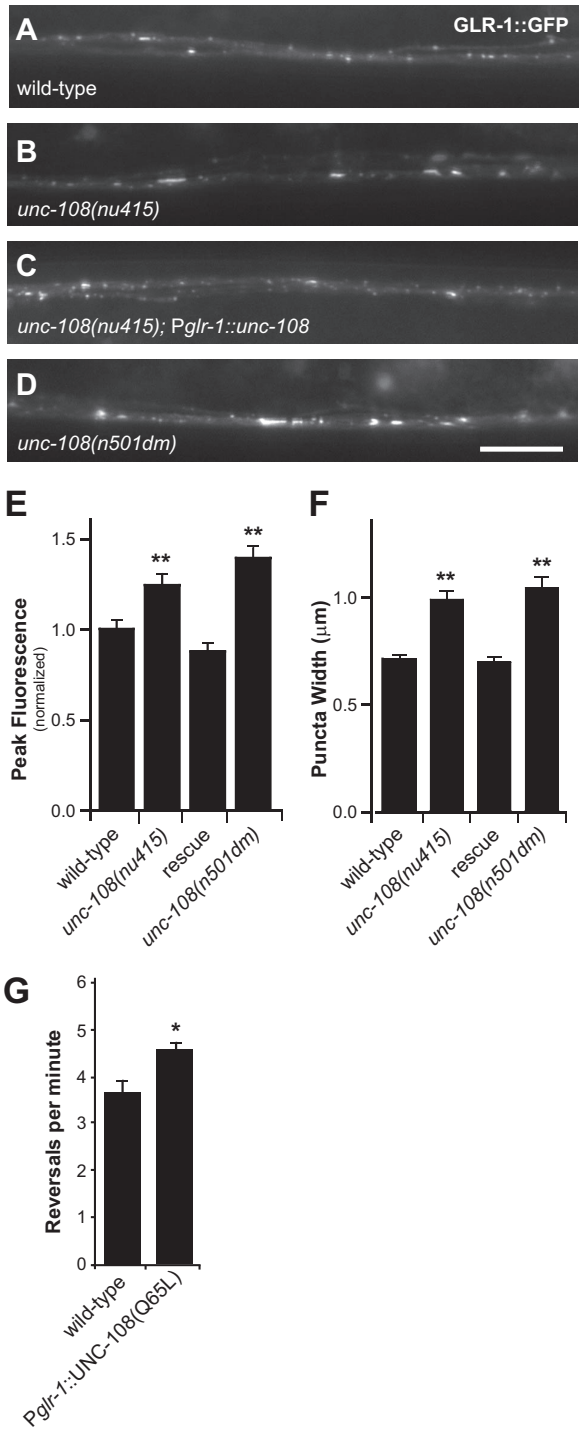

Figure 2. UNC-108/Rab2 functions in the ventral cord to regulate the abundance of GLR-1::GFP. (A–D) GLR-1::GFP puncta in the anterior ventral nerve cord of stage four larval (L4) wild type (A), *unc-108(nu415)* (B), rescued *unc-108(nu415)* (C), and *unc-108(n501dm)* gain-of-function (D) animals were imaged. The increased GLR-1:GFP puncta intensities and widths in *unc-108(nu415)* mutants were rescued by the expressing FLAG-tagged UNC-108 with the *glr-1* promoter (C). (E–F) Puncta intensities, measured as peak fluorescence (normalized to wild type animals) (E), and widths (F) were compared in wild type (n = 37), *unc-108(nu415)* (n = 35), rescued *unc-108(nu415)* (n = 32), and *unc-108(n501dm)* animals (n = 30). (G) Reversal frequencies were assayed for wild-type animals (n = 25) and animals expressing P*glr-1*::UNC-108(Q65L) (n = 25). *unc-108(nu415)* animals show an increase in reversal frequency compared with wild-type controls ($p = 0.0125$). Bar, 10 μm, error bars represent SEM, and values that differ significantly from wild type (by Student's *t* test) are indicated as follows: *$p < 0.05$ and **$p < 0.001$.

ferase binding (Rak *et al*., 2003; Pfeffer, 2005). The uncoordinated locomotion defect of *unc-108(nu415)* animals was rescued by the expression of FLAG-tagged UNC-108 in all neurons (using the *snb-1* promoter) (Figure 1C). Rescue was not observed when *unc-108* was expressed in cholinergic neurons, ventral cord interneurons, or in body muscles. Consistent with function in neurons, an *unc-108* transcriptional reporter construct (P*unc-108*::GFP) was expressed strongly in many, and perhaps all neurons (Figure 1D). Weaker expression was also observed in the gut, seam cells, and hypodermis. Finally, *unc-108(nu415)* mutants were slightly hypersensitive to the paralytic effects of aldicarb, an acetylcholinesterase inhibitor (Supplemental Figure S1), a phenotype that is often associated with changes in synaptic transmission at neuromuscular junctions (Miller *et al*., 1996; Loria *et al*., 2004; Sieburth *et al*., 2005). Collectively, these results argue that UNC-108 acts in neurons to promote normal locomotion.

The *unc-108* gene was originally defined by two gain-of-function alleles (*n501dm* and *n777dm*), both of which cause a dominantly inherited uncoordinated locomotion phenotype (Park and Horvitz, 1986). Both dominant *unc-108* alleles are predicted to increase the abundance of GTP-liganded Rab2. The *n501dm* (D122N) and *n777dm* (S149F) mutations alter conserved residues in the GTPase domain (Simmer *et al*., 2003) (Figure 1A). A dominant-negative missense mutation in the corresponding residue of Ras increases the spontaneous guanine nucleotide exchange rate, thereby producing a constitutively active Ras protein (Cool *et al*., 1999). The S149 residue is conserved among most Ras related GTPases and falls in the G5 loop, which is also required for guanine nucleotide binding (Paduch *et al*., 2001). To confirm the gain-of-function nature of these alleles, we expressed mutant *unc-108*/Rab2 cDNAs containing these mutations, and we found that both produced an uncoordinated locomotion phenotype similar to that seen in the *unc-108(dm)* mutants (data not shown).

Together, these results suggest that the *unc-67* and *unc-108* genes are allelic, and that gain and loss-of-function *unc-108* alleles produce similar locomotion defects. Previous studies showed that the function of Rab proteins in intracellular membrane fusion requires GTP hydrolysis (Walworth *et al*., 1992); therefore, it was not surprising that similar locomotion defects were produced by gain and loss-of-function *unc-108* mutations. Hereafter, we refer to this gene as *unc-108*/Rab2.

UNC-108/Rab2 Regulates GLR-1 Distribution in the Ventral Nerve Cord

In *unc-108(nu415)* mutants, significant increases were observed in the intensity (24% increase, $p < 0.001$) and width (41% increase, $p < 0.001$) of GLR-1::GFP puncta in the ventral nerve cord (Figure 2, A and B, and E and F) We showed previously that GLR-1::GFP puncta correspond to receptors clustered at postsynaptic elements (Rongo *et al*., 1998; Burbea *et al*., 2002). A similar increase in GLR-1::GFP fluorescence was also observed in *unc-108(n501dm)* and *unc-108(e713)* mutants, although the defects caused by *e713* were less severe (Figure 2, D–F; data not shown). Thus, similar changes in GLR-1::GFP distribution were observed in both

loss and gain-of-function *unc-108* mutants, as was the case for the locomotion defects. The increased GLR-1::GFP punctal fluorescence in *unc-108(nu415)* mutants was rescued by expression of a FLAG-tagged UNC-108 construct under the *glr-1* promoter (Figure 2C, E, and F), demonstrating that UNC-108/Rab2 activity in ventral cord interneurons is required for proper localization of GLR-1::GFP. An anti-FLAG antibody detected a 23-kDa protein in extracts of transgenic animals, which is consistent with the predicted molecular weight for the UNC-108::FLAG protein (Supplemental Figure S2A). FLAG-tagged UNC-108 was expressed in *glr-1* interneurons, and immunostaining of animals expressing this construct indicated that UNC-108::FLAG is diffusely distributed in neurites, with occasional small puncta (Supplemental Figure S2, B and C). The total abundance of GLR-1::GFP in *unc-108(nu415)* mutants and wild-type controls were not significantly different (wild type 24.8 ± 6.0 AU vs. *unc-108* 24.5 ± 4.4 AU, $p = 0.57$) (Figure 3A), suggesting that changes in GLR-1::GFP puncta fluorescence observed in *unc-108* mutants were unlikely to be caused by changes in total GLR-1 abundance.

To determine whether UNC-108 regulates the function of endogenously expressed GLR-1 receptors, we examined the effect of UNC-108 on a GLR-1–dependent behavior. The frequency of reversals during spontaneous locomotion can be utilized as a behavioral assay for GLR-1 function. Previous studies have shown that mutants with increased glutamatergic signaling have higher reversal frequencies compared with wild-type control animals (Zheng *et al*., 1999; Burbea *et al*., 2002; Juo and Kaplan, 2004, Schaefer and Rongo, 2006; Juo *et al*., 2007). The uncoordinated locomotion of *unc-108(nu415)* mutants precludes their use in a reversal assay; therefore, we used transgenic animals expressing a GTPase-defective mutant UNC-108(Q65L) in the ventral cord interneurons. Animals expressing UNC-108(Q65L) had significantly higher reversal frequencies compared with wild-type controls (Figure 2G), consistent with increased glutamatergic signaling. Thus, UNC-108 regulates both GLR-1::GFP abundance in the ventral cord, and produces corresponding changes in a GLR-1–mediated behavior.

To determine whether UNC-108/Rab2 regulates the trafficking of other synaptic proteins, we examined the distribution of a GFP-tagged synaptic vesicle protein, Synaptobrevin (GFP::SNB-1) in the ventral cord interneurons. We found that neither the GFP::SNB-1 punctal fluorescence nor the diffuse axon fluorescence were altered in *unc-108(nu415)* mutants (Figure 3B-E). We also analyzed several other presynaptic markers in ventral cord motor neurons (including SYD-2/α-Liprin, UNC-10/RIM-1, SNN-1/Synapsin, Gelsolin, and INS-22/Insulin), and we found that all were distributed in a normal pattern in *unc-108* mutants (data not shown). Thus, UNC-108/Rab2 is not generally required for trafficking of synaptic proteins, nor is it required for normal synapse formation or synapse morphology. Instead, these results suggest that UNC-108/Rab2 plays a relatively specific role in the trafficking of a subset of synaptic proteins, including GLR-1.

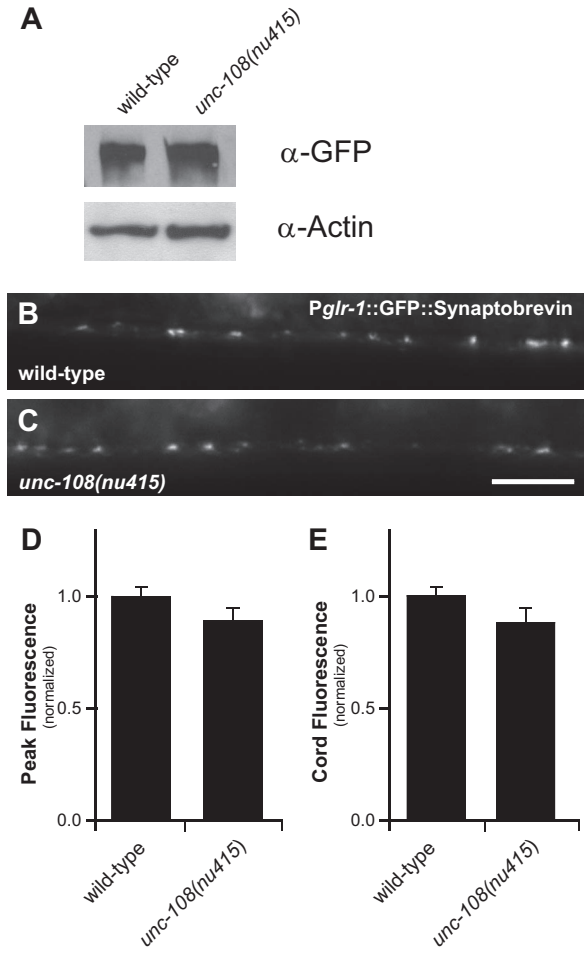

Figure 3. UNC-108/Rab2 does not alter the expression of GLR-1::GFP or the trafficking of SNB-1::GFP. (A) Quantitative western blots against GLR-1::GFP, by using an anti-GFP antibody, were performed on wild type, *unc-108(nu415)* worm lysates. Actin was used for normalization. The total abundance of GLR-1::GFP in *unc-108(nu415)* mutants ($n = 5$) and wild-type controls ($n = 5$) were not significantly different (wild type 24.8 ± 6.0 AU vs. *unc-108* 24.5 ± 4.4 AU, $p = 0.57$). (B and C) Representative images of GFP-tagged synaptobrevin expression in the ventral nerve cord under the *glr-1* promoter in stage 4 larval (L4) wild-type (B) and *unc-108(nu415)* (C) mutant animals. (D and E) The puncta intensities (D) and diffuse cord fluorescence (E) (both normalized to wild type) were measured in the indicated number of animals: wild type ($n = 36$) and *unc-108(nu415)* ($n = 38$). There was no statistically significant difference in peak or cord fluorescence (by Student's *t* test, $p = 0.797$ and 0.402, respectively) between *unc-108(nu415)* and wild type animals. Bar, 10 μm; error bars represent SEM.

UNC-108/Rab2 Is Not Required for ER Retention of KDEL-containing Proteins

To determine the mechanism for the altered trafficking of GLR-1::GFP in *unc-108* mutants, we first tested the known secretory functions of Rab2. Previous studies in mammalian systems suggested that Rab2 plays an important role in retrograde trafficking between the Golgi and the ER (Tisdale and Balch, 1996). To assay COPI-mediated retrograde transport, we expressed a secreted form of YFP (ssVenus) containing the ER retention signal KDEL (ssVenus::KDEL). Proteins containing the KDEL retention signal are constitutively retrieved from the Golgi by COPI-mediated retrograde transport, resulting in their retention in the ER (Pidoux and Armstrong, 1992; Terasaki *et al*., 1996). In PVC interneuron cell bodies, ssVenus::KDEL was localized in a diffuse network consistent with retention in the ER in both wild-type and *unc-108(nu415)* mutants (Figure 4, A and B). In both wild type and *unc-108* neurons, the ssVenus::KDEL signal did not colocalize with the Golgi marker RFP::GOS-28 (Volchuk *et al*., 2004) (Figure 4, E and F). Mutations that disrupt COPI-mediated transport often alter the morphology of the ERGIC (Donaldson *et al*., 1990; Guo *et al*., 1994; Gaynor and

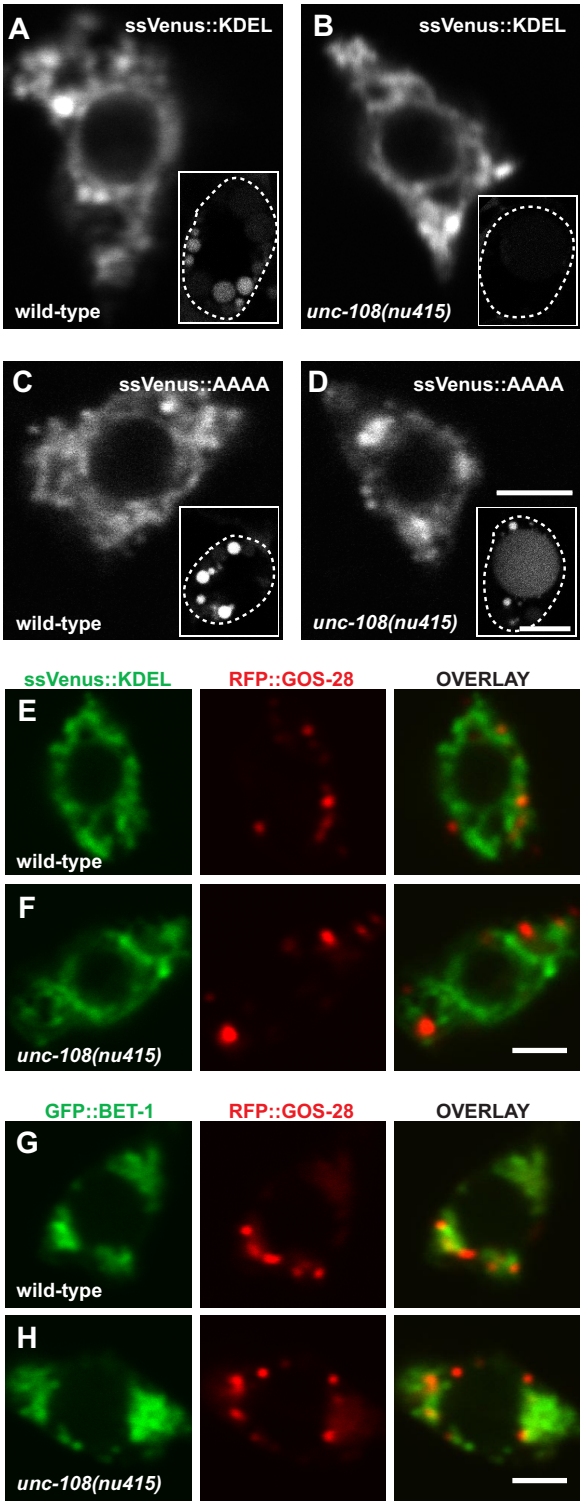

Figure 4. UNC-108/Rab2 is not required for ER retention of KDEL-containing proteins. (A and B) A translational fusion construct containing a secreted form of Venus fused to a KDEL ER retention signal (ssVenus::KDEL) under the *glr-1* promoter, was expressed in L4 wild-type (A) and *unc-108(nu415)* mutant animals (B), and confocal images of the PVC neuron cell bodies and of the coelomocytes (inset images) were taken. Single coelomocyte cell bodies are outlined by dashed lines. (C and D) ssVenus::AAAA was imaged in neuronal cell bodies and coelomocytes (inset) of wild-type (C) and *unc-108(nu415)* mutant (D) worms. Neuronal cell body images of ssVenus::AAAA expression were imaged at a higher laser intensity (710V) compared with ssVenus::KDEL (510V) to account for the dimmer fluorescence of the secreted ssVenus::AAAA. Coelomocytes images were imaged at the same laser intensity for all genotypes. (E and F) The localization pattern of ssVenus:KDEL in comparison with the Golgi marker RFP::GOS-28 was examined in wild type (E) and *unc-108(nu415)* mutant (F) neuronal cell bodies. No colocalization of ssVenus::KDEL and RFP::GOS-28 was observed in wild-type or *unc-108* mutant worms. (G and H) The morphology of the GFP::BET-1-labeled pre-Golgi intermediate compartment (ERGIC) and its colocalization pattern with RFP::GOS-28 in wild-type (G) and *unc-108(nu415)* mutant neuronal cell bodies was imaged. There was no change in GFP::BET-1 localization in *unc-108* mutants compared with wild-type controls. Bars, 2 μm (cell bodies) and 5 μm (coelomocytes, inset images).

Emr, 1997); however, the morphology of the ERGIC (labeled with RFP::BET-1, Volchuk *et al.*, 2004) was unaltered in *unc-108* mutants (Figure 4, G and H).

In yeast, mutations that disrupt COPI function often result in secretion of KDEL-containing ER proteins, e.g., Kar2/BiP (Semenza *et al.*, 1990; Andag *et al.*, 2001). Therefore, as an independent measure of ER retention, we analyzed secretion of ssVenus::KDEL. Secreted fluorescent proteins are endocytosed and degraded by coelomocytes, which are macrophage-like scavenger cells in the body cavity (Fares and Greenwald, 2001; Sieburth *et al.*, 2007; Speese *et al.*, 2007). Thus, failure to retain ssVenus::KDEL in the ER should result in its secretion by interneurons, which can be detected as fluorescence in postendocytic structures of coelomocytes. ssVenus::KDEL fluorescence was dim in the coelomocytes of both wild-type and *unc-108(nu415)* mutants (Figure 4, A and B inset). In fact, decreased coelomocyte ssVenus::KDEL fluorescence was observed in *unc-108(nu415)* mutants, which is likely due to a defect in postendocytic trafficking in coelomocytes (detailed below). As expected, proteins lacking ER retention signals (e.g., ssVenus::AAAA) were efficiently secreted from both *unc-108(nu415)* mutants and wild-type interneurons (Figure 4, C and D, inset). Collectively, these results suggest that COPI-mediated retrograde transport remains functional in *unc-108* mutants, although we cannot exclude a modest defect in this pathway.

Anterograde Trafficking Occurs Normally in unc-108/Rab2 Mutants

Disrupting Rab2 function in cultured mammalian cells is also associated with defects in anterograde transport of cargo proteins, e.g., VSV-G (Tisdale and Balch, 1996). Similar anterograde trafficking defects are often observed in yeast mutants with disrupted COPI retrograde transport (Gaynor and Emr, 1997). Therefore, we did several experiments to test the idea that the altered distribution of GLR-1::GFP in *unc-108* mutants was caused by anterograde trafficking defects. GLR-1::GFP accumulated in the ventral cord of *unc-108* mutants, suggesting that anterograde trafficking out of the cell body occurs normally in these mutants. If early secretory components (e.g., ER or Golgi membranes) were mislocalized to the ventral cord in *unc-108* mutants, this could account for the altered GLR-1::GFP distribution in these mutants. However, we did not find increased ventral cord abundance for several ER and Golgi markers in *unc-108* mutants, including ssVenus::KDEL, BET-1 (ERGIC), Syntaxin-5 (TGN), and Syntaxin-16 (TGN) (Figure 5, A–D; data not shown). Mutations disrupting COPII-mediated anterograde transport in yeast often result in accumulation of ER membranes (Kaiser and Schekman, 1990). Again, we did not observe any obvious change in the ER network, as visualized by ssVenus::KDEL (Figure 4, A and B).

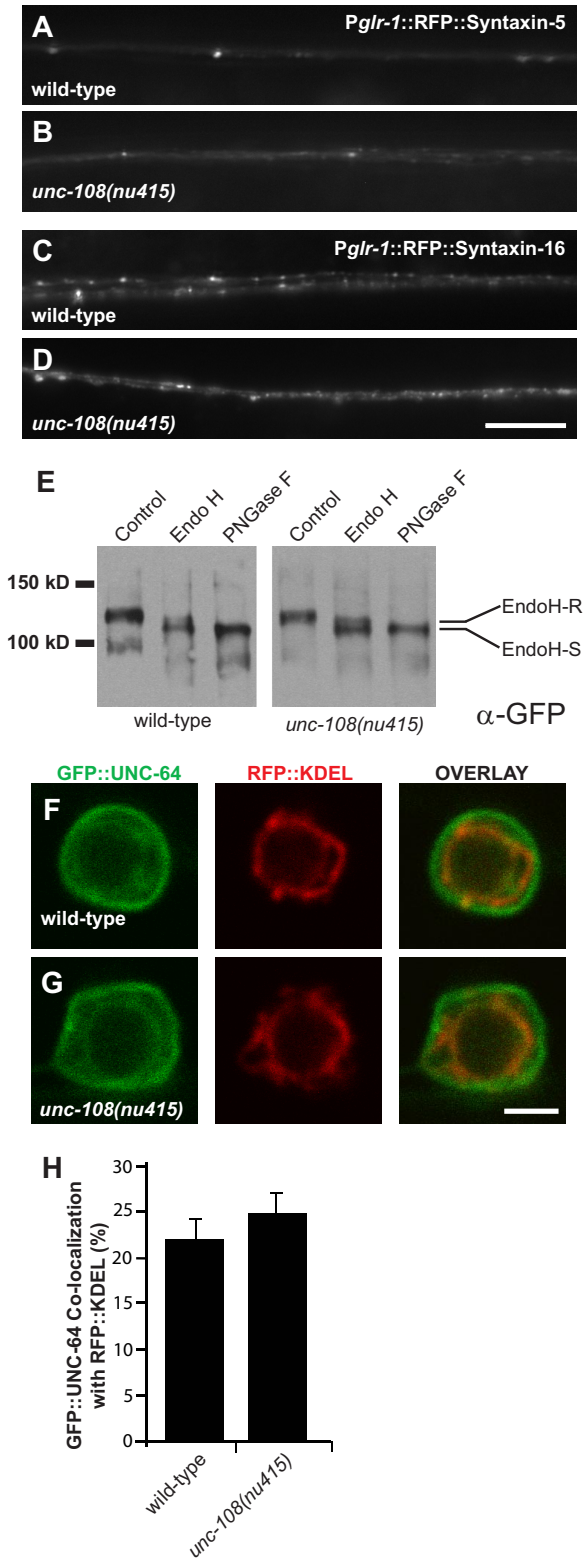

Figure 5. Anterograde trafficking occurs normally in *unc-108*/Rab2 mutants. (A and B) L4 Animals expressing RFP::Syntaxin-5 in the ventral cord interneurons, under the *glr-1* promoter in wild type (A) or *unc-108(nu415)* (B) Animals were imaged. No difference in RFP::Syntaxin-5 localization in the ventral nerve cord was observed in *unc-108(nu415)* mutant animals compared with wild-type controls. (C and D) L4 animals expressing RFP::Syntaxin-16, under the *glr-1* promoter in wild-type (C) or *unc-108(nu415)* (D) animals were imaged. No difference in RFP::Syntaxin-16 localization in the ventral nerve cord was observed in *unc-108(nu415)* mutant animals compared with wild-type controls. (E) Endo H assays and a subsequent quantitative western blot (against GLR-1::GFP by using an anti-GFP antibody) of wild-type and *unc-108(nu415)* mutant worm lysates. The control lane contained no enzyme and PNGase F was used as a control for the complete removal of N-linked glycosylations from GLR-1::GFP. In wild type animals, 65 ± 2.3% of GLR-1::GFP was Endo H-sensitive (n = 5). In *unc-108(nu415)* animals, 58 ± 4.6% of was Endo H sensitive (n = 5) (EndoH-R, Endo H resistant; EndoH-S, Endo H sensitive). (F and G) Representative confocal images of colocalization between GFP::UNC-64 and RFP::KDEL used the *unc-129* promoter in wild-type (F) and *unc-108(nu415)* (G) neuronal cell bodies. (H) Colocalization between GFP::UNC-64 and RFP::KDEL was quantified for wild type (n = 10) and *unc-108(nu415)* mutants (n = 10), and no statistically significant difference was found (by Student's *t* test, p = 0.194). Bars, 10 μm (ventral nerve cord) and 2 μm (cell bodies); error bars represent SEM.

To more directly assay anterograde transport, we analyzed glycosylation of GLR-1::GFP. Anterograde delivery of GLR-1 to the Golgi can be determined by analyzing sensitivity to the endoglycosidase Endo H (Grunwald and Kaplan, 2003). Endo H removes *N*-glycans containing immature carbohydrate chains, which are typically found in the ER. In the Golgi, carbohydrate chains undergo further modifications, rendering them resistant to Endo H. The Endo H-sensitive fractions of GLR-1::GFP observed in wild-type (65%, SEM ± 2.3%) and *unc-108(nu415)* mutants (58%, SEM ± 4.6%) were similar (Figure 5E), suggesting that anterograde delivery of GLR-1::GFP to the Golgi occurs normally in *unc-108* mutants.

Finally, we also examined anterograde transport of the plasma membrane SNARE Syntaxin-1 (encoded by *unc-64*). In both wild type and *unc-108* mutants, GFP-tagged UNC-64 expressed in PVC interneurons was found both in intracellular membranes, and at the periphery of the cell body, which likely corresponds to the plasma membrane. We found that the extent of colocalization of GFP::UNC-64 with ssTomato::KDEL was not significantly different in *unc-108* mutants compared with wild-type controls (Figure 5, F–H), suggesting that UNC-64 was not retained in the ER in these mutants. Collectively, these results suggest that *unc-108* mutants do not have a significant defect in anterograde transport.

GLR-1::GFP Accumulates in Endosomal Structures in unc-108/Rab2 Mutants

To further address the nature of the trafficking defect observed in *unc-108* mutants, we analyzed the distribution of GLR-1::GFP in neuronal cell bodies. We found that GLR-1::GFP also had an aberrant distribution in interneuron cell bodies of *unc-108(nu415)* and *unc-108(n501dm)* mutants (Figure 6, A–C). In both *unc-108* mutants, GLR-1::GFP accumulated in large tubulovesicular structures that were observed infrequently in wild-type neurons. The tubulovesicular structures had very bright GLR-1::GFP pixel intensities (corresponding to the brightest ~5% of pixels in each cell) (Supplemental Figure S4, B, D, and E). By contrast, wild-type neurons lacked these tubulovesicular structures, and they had fewer pixels with high GLR-1::GFP intensities (Supplemental Figure S4, A, C, and E). Thus, in *unc-108* mutant neurons, there was an accumulation of GLR-1::GFP in these aberrant structures.

To characterize the tubulovesicular structures, we determined whether they colocalized with several RFP-tagged proteins that label specific organelles. Because the tubulove-

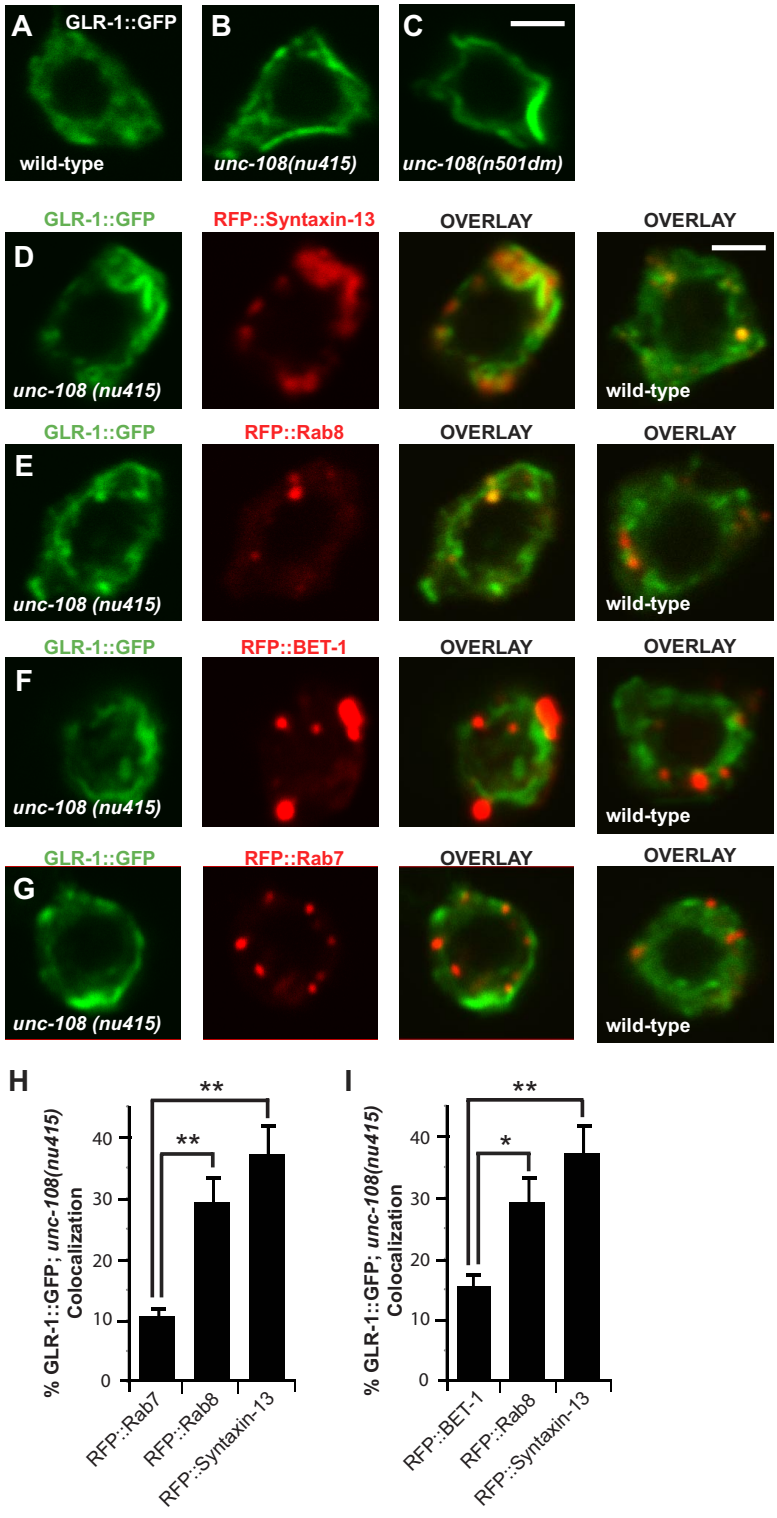

Figure 6. *unc-108(nu415)* mutants have accumulations of GLR-1:GFP in neuronal cell bodies that colocalize with endosomal marker proteins. (A–G) Confocal images of interneuron cell bodies are shown in the indicated genotypes. A single plane is shown for each cell. (A–C) GLR-1::GFP distribution is shown in wild-type (A), *unc-108(nu415)* (B), and *unc-108(n501dm)* (C) worms. (D–G) Individual red and green channel and overlay images of interneuron cell bodies coexpressing GLR-1::GFP and RFP::Syntaxin-13 (D), RFP::Rab8 (E), RFP::BET-1 (F), or RFP::Rab7 (G) in *unc-108(nu415)* mutants. Overlay images of GLR-1::GFP and the RFP-tagged markers in neuronal cell bodies in wild-type animals are also shown (D–G). (H and I) Quantification of GLR-1::GFP colocalization with RFP::Syntaxin-13, RFP::Rab8, RFP::BET-1, and RFP::Rab7 in *unc-108(nu415)* mutants. Graphs showing the percent GLR-1::GFP colocalization with RFP::Rab7 (H) and RFP::BET-1 (I) compared with colocalization with RFP::Rab-8 and RFP::Syntaxin-13 are presented. There is a statistically significant increase in GLR-1::GFP colocalization with RFP::Rab8 and RFP::Syntaxin-13 compared with RFP::Rab7 (p values = 4.0793×10^{-4} and 4.79×10^{-5} respectively) and RFP::BET-1 (p values = 0.0033 and 2.43×10^{-4}, respectively) in *unc-108(nu415)* neuronal cell bodies. Quantification of colocalization of GLR-1::GFP with the RFP-tagged compartment markers are described in detail in *Materials and Methods* and Supplemental Figure S4. Bars, 2 μm. Error bars represent SEM, and values that differ significantly from wild type (by Student's *t* test) are indicated as follows: *$p < 0.01$ and **$p < 0.001$.

sicular structures correspond to the brightest pixels in each cell, we analyzed colocalization of RFP-tagged proteins only for the brightest GLR-1::GFP pixels. The threshold GFP pixel intensity utilized for this analysis was one SD lower than the mean value in the tubulovesicular structures (Supplemental Figure S4D). In this manner, we showed that GLR-1::GFP in these aberrant structures was significantly colocalized with the endosomal markers RFP::Syntaxin-13 and RFP::Rab8, but it was not significantly colocalized with RFP::Bet-1 (ERGIC), and RFP::Rab7 (late endosomes) (Figure 6, D–I). Using the same intensity thresholds, the brightest GFP pixels showed significantly less colocalization with RFP::Syntaxin-13 and RFP::Rab8 in wild-type neurons than in *unc-108(nu415)* neurons (Supplemental Figure S5, A–F). The dim diffuse GLR-1::GFP staining observed in both wild-type and *unc-108* mutant neurons was significantly colocalized with

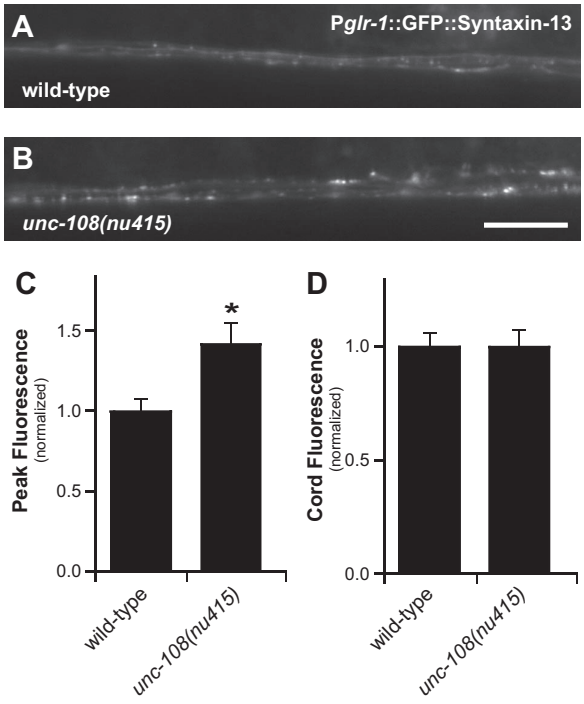

Figure 7. *unc-108(nu415)* mutants have accumulated GFP::Syntaxin-13. (A and B) GFP::Syntaxin-13 puncta in the anterior ventral nerve cords of wild-type (A) and *unc-108(nu415)* animals (B). Puncta intensities (C) and diffuse cord fluorescence (D) (both normalized to wild type) were compared in wild-type (n = 42) and *unc-108(nu415)* (n = 38) animals. There was a 42% increase in peak fluorescence in *unc-108(nu415)* mutants ($p = 0.00279$) compared with wild-type controls, and no statistically significant difference in cord fluorescence. *$p < 0.01$, by Student's *t* test. Bar,10 μm; error bars represent SEM.

ssTomato::KDEL, consistent with our estimate that ~65% of GLR-1::GFP is retained in the ER based on Endo H sensitivity assays (Grunwald and Kaplan, 2003) (Supplemental Figure S5, G–I). A panel of other RFP-tagged intracellular compartment markers were examined for colocalization with GLR-1::GFP in *unc-108(nu415)* mutant neurons, including Rab14, Rab11, Rab10, GOS-28, and Syntaxin-16, but none were significantly colocalized with GLR-1::GFP (Supplemental Figure S3). Together, these results suggest that GLR-1::GFP accumulates in abnormal endosomal derivatives in *unc-108* mutants.

In addition to the cell body, we also expect to find endosomal structures in neuronal processes. Therefore, we analyzed the distribution of an endosomal marker (GFP::Syntaxin-13) in the ventral cord, after transgenic expression in the ventral cord interneurons or in the cholinergic DA motor neurons (using the *glr-1* or *unc-129* promoter, respectively). In both cases, we found that the intensity of GFP::Syntaxin-13 puncta in the ventral cord significantly increased in *unc-108(nu415)* mutants compared with wild-type controls (Figure 7, A–D; data not shown). This further supports the conclusion that there is an endosomal trafficking defect in *unc-108(nu415)* mutant neurons.

UNC-108/Rab2 Plays a Role in Postendocytic Trafficking in Coelomocytes

To verify that UNC-108/Rab2 has a postendocytic function, we analyzed the morphology of the endosomal/lysosomal pathway in coelomocytes. We microinjected a fluid-phase endocytosis marker TR-BSA into the body cavity of adult worms that express RME-8::GFP, which labels the limiting membrane of endosomes (Zhang *et al*., 2001). Postendocytic trafficking of TR-BSA in coelomocytes was monitored at sequential time points (Figure 8). In wild-type animals, internalized TR-BSA was observed in primarily RME-8::GFP–positive vesicles 10 min after injection, whereas after 30 min, TR-BSA was observed increasingly in RME-8::GFP-negative

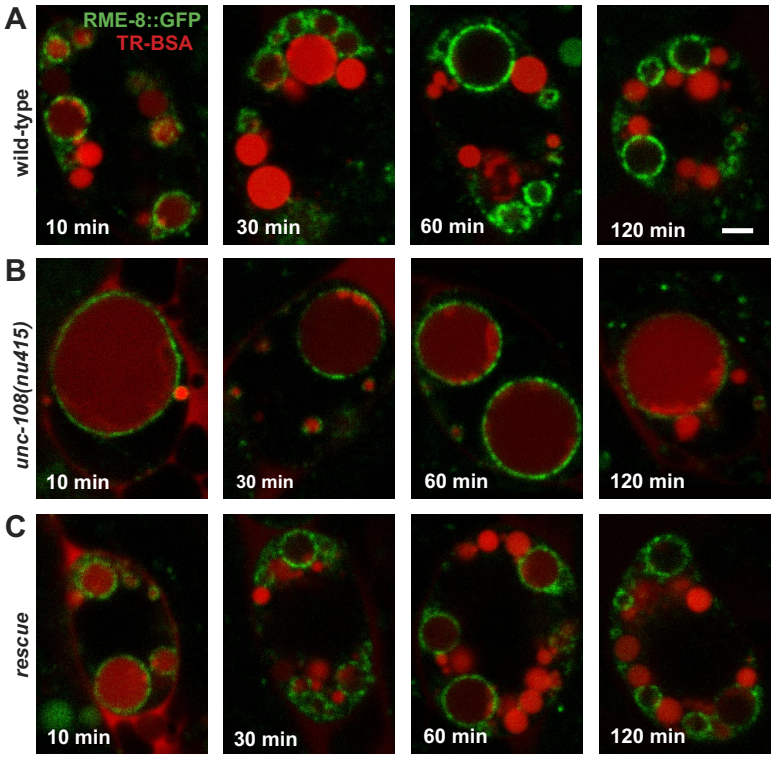

Figure 8. *unc-108(nu415)* mutants have altered postendocytic trafficking in coelomocytes. TR-BSA was injected into the pseudocoelom of worms expressing RME-8::GFP to measure endocytosis and postendocytic trafficking over a time course. Single-plane confocal images of individual coelomocytes in wild type (A) and *unc-108(nu415)* (B) 10, 30, 60, and 120 min after TR-BSA injections. (C) *unc-108(nu415)* mutants were rescued by the expression of UNC-108::FLAG under the coelomocyte-specific promoter *unc-122*, injected with TR-BSA, and imaged at 10, 30, 60, and 120 min. Five animals for each genotype were imaged, and representative images were chosen. Bar, 2 μm.

vesicles, which presumably correspond to late endosomes and lysosomes (Zhang *et al*., 2001). If in *unc-108(nu415)* mutant animals, endocytosis occurs normally, but a postendocytic trafficking step is disrupted, you would expect to see changes in the size or distribution of endosomal compartments in the coelomocytes of these animals. In fact, in *unc-108(nu415)* mutants, there was a significant reduction in the number of RME-8::GFP–positive intracellular vesicles, but each vesicle was significantly larger than those observed in wild-type controls. In addition to this change in the morphology of the RME-8–containing vesicles, TR-BSA trafficking into RME-8::GFP–negative vesicles was significantly delayed in *unc-108(nu415)* mutants. 60 min after injection, TR-BSA was visible only in RME-8::GFP–positive vesicles of *unc-108(nu415)* mutant coelomocytes, eventually becoming visible in RME-8::GFP negative vesicles at 120 min (Figure 8B). Trafficking defects seen in *unc-108(nu415)* mutants were rescued by expression of FLAG-tagged UNC-108 by using the coelomocyte-specific *unc-122* promoter (Loria *et al*., 2004) (Figure 8C). These results demonstrate that UNC-108/Rab2 is required for postendocytic trafficking in coelomocytes, and specifically for endosome-to-lysosome trafficking. A similar coelomocyte post-endocytic trafficking defect was recently described in mutants carrying a dominant *unc-108* allele, and after knockdown of *unc-108* by RNAi (Lu *et al*., 2008). These results are also consistent with the observed trafficking defects in ventral cord interneurons: accumulation of GLR-1::GFP in an endosomal compartment in cell bodies, and altered distribution of the endosomal marker Syntaxin-13 in the ventral cord.

UNC-108/Rab2 Is Not Required for Ubiquitin-mediated Endocytosis and Degradation of GLR-1

Thus far, our results suggest that the accumulation of GLR-1::GFP in the ventral cord results from a defect in postendocytic trafficking in *unc-108* mutants. We have shown previously that GLR-1::GFP undergoes ubiquitin-mediated postendocytic degradation (Burbea *et al*., 2002). Overexpression of Myc-tagged ubiquitin (MUb) in the ventral cord interneurons results in the formation of MUb–GLR-1 conjugates and decreased density of GLR-1::GFP puncta in the ventral cord (Burbea *et al*., 2002). The effect of MUb on GLR-1::GFP puncta density was prevented by mutations that block endocytosis (e.g., *unc-11* AP180 mutations) (Burbea *et al*., 2002). In other systems, ubiquitin-promoted degradation of membrane proteins is mediated by targeting ubiquitin-conjugates to the internalized vesicles of multivesicular bodies (MVBs) (Katzmann *et al*., 2001; Bilodeau *et al*., 2003). To further characterize MUb-mediated degradation of GLR-1, we tested the role of the MVB sorting pathway in this process. The VPS-4 AAA ATPase is required for internalizing cargo from the limiting membrane of endosomes to the internalized vesicles of MVBs (Babst *et al*., 2002; Yeo *et al*., 2003). As expected, expressing a dominant-negative VPS-4 mutant, *vps-4*(DN), significantly decreased the effects of MUb on the density of GLR-1::GFP puncta (Figure 9, A–E). These results indicate that GLR-1, like other membrane proteins, undergoes post-endocytic degradation by ubiquitin-mediated sorting into the MVB pathway.

If UNC-108/Rab2 were required for ubiquitin-mediated degradation of GLR-1, this would explain the accumulation

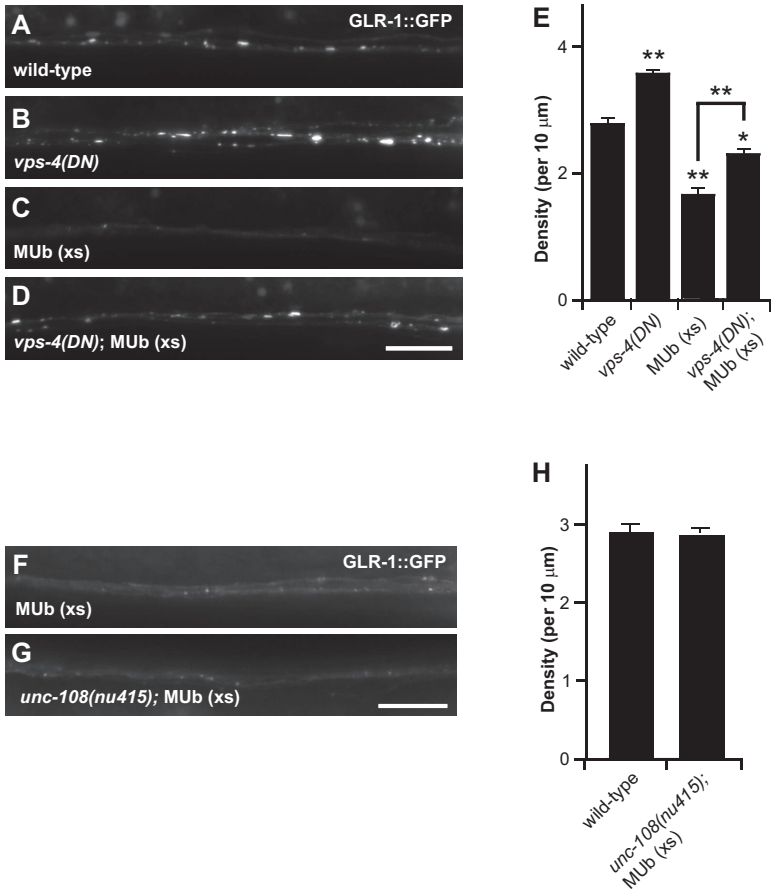

Figure 9. The *unc-108(nu415)* mutation does not suppress the effects of overexpressed ubiquitin on GLR-1::GFP. (A–D) GLR-1::GFP puncta in the anterior ventral nerve cord of L4 wild-type (A), *vps-4*(DN) (B), MUb (C), and *vps-4*(DN);MUb (D) animals were imaged. (E) GLR-1:GFP puncta density was quantified in wild-type (n = 34), *vps-4*(DN) (n = 40), MUb (n = 28), and *vps-4*(DN);MUb (n = 39) animals. (F and G) GLR-1::GFP puncta in anterior ventral cords of MUb (F) and *unc-108(nu415);*MUb (G) animals. (H) GLR-1::GFP puncta density in MUb (n = 30) and *unc-108(nu415);* MUb (n = 30) animals were not significantly different ($p = 0.72$). Error bars represent SEM, and values that differ significantly from wild type (by Student's *t* test) are indicated as follows: *$p < 0.01$ and **$p < 0.001$. Bar, 10 μm.

of GLR-1::GFP in *unc-108* mutants. We did several experiments to test this possibility. First, unlike *vps*-4(DN), the *unc-108(nu415)* mutation had no effect on the MUb-induced decrease in GLR-1::GFP puncta density (Figure 9, F–H). Second, we compared the effects of the *vps*-4(DN) and the *unc-108(nu415)* mutations on the distribution of GLR-1::GFP in the cell bodies of ventral cord interneurons. Expression of *vps*-4(DN) is predicted to prevent internalization of proteins from the limiting membrane to internalized vesicles of MVBs (Babst *et al*., 2002; Yeo *et al*., 2003). Consistent with this prediction, GLR-1::GFP accumulated in the limiting membrane of large vesicular structures in PVC cell bodies of *vps*-4(DN) mutants (Figure 10B). By contrast, in *unc-108(nu415*) mutants, GLR-1::GFP accumulated in tubulovesicular structures in PVC interneuron cell bodies (Figures 6, B and C, and 10C). Thus, VPS-4 and UNC-108 had distinct effects on the distribution of GLR-1::GFP in cell bodies. Together, these results suggest that UNC-108/Rab2 is not required for ubiquitin-mediated sorting of GLR-1::GFP into the MVB pathway.

UNC-108/Rab2 Defines an Endocytic Pathway That Acts in Parallel to the MVB Pathway

Previous studies have shown that after internalization GluRs are sorted into multiple, independent postendocytic pathways (Ehlers, 2000; Lin *et al*., 2000). If this were the case for GLR-1, then one might expect that GLR-1 could be subject to endocytosis by both the ubiquitin/MVB pathway, and by additional endocytic pathways which may require UNC-108/Rab2. To test this idea, we examined the distribution of GLR-1::GFP in *vps*-4(DN)*; unc-108(nu415)* double mutants. If UNC-108/Rab2 and the MVB pathway define two alternative recycling mechanisms regulating GLR-1, then we would expect that these mutations would have additive effects. The distribution of GLR-1::GFP in PVC interneuron cell bodies in *vps*-4(DN)*; unc-108(nu415)* double mutants seemed different from that of either single mutant (Figure 10, B–D) suggesting possible additivity. In the ventral cord, GLR-1::GFP puncta fluorescence in *vps-4*(DN)*; unc-108(nu415)* double mutants was significantly greater than that observed in either single mutant (Figure 10, F–J), demonstrating that these mutations had additive effects on GLR-1::GFP. These results suggest that UNC-108/Rab2 and VPS-4 define two parallel pathways that regulate postendocytic trafficking of GLR-1.

DISCUSSION

Rab proteins play important roles in trafficking of vesicles and in determining specificity of vesicle fusion within the cell (Zerial and McBride, 2001; Grosshans *et al*., 2006). UNC-108 is more similar to RAB-2 (87% identical to mouse Rab2) than any other *C. elegans* Rab protein. Thus, this study represents the first analysis of a Rab2 loss-of-function phenotype in a metazoan.

A New Function for Rab2: UNC-108 Promotes Postendocytic Trafficking

We showed that UNC-108/Rab2 is required for postendocytic trafficking in both neurons and coelomocytes. In coelomocytes, uptake of Texas Red-BSA was normal, but there was a decreased rate of trafficking from RME-8::GFP–positive endosomes to later endocytic compartments. The decreased rate in endosome to lysosome traffic leads to the enlargement of the RME-8::GFP–positive endosomes. Similar coelomocyte trafficking defects were recently described in mutants carrying a dominant *unc-108* allele, and after knockdown

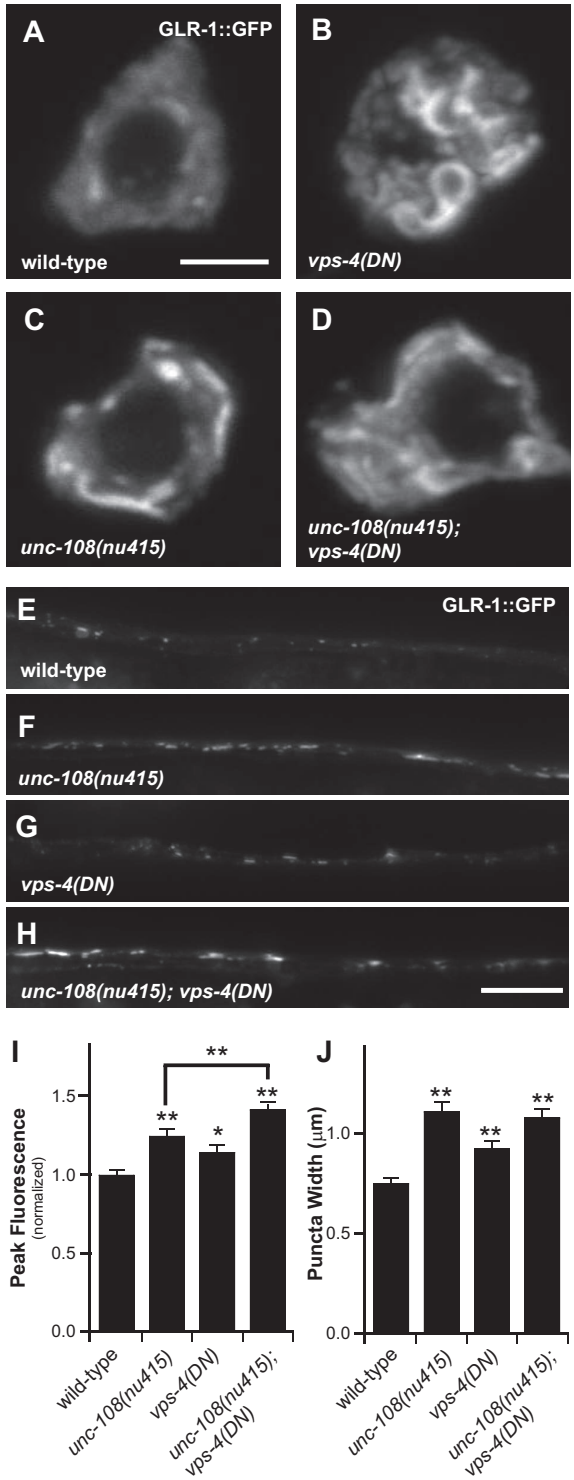

Figure 10. *unc-108(nu415)* and *vps-4(DN)* mutations have additive effects on GLR-1::GFP. (A–D) Confocal images of GLR-1::GFP distribution in PVC interneuron cell bodies in wild type (A), *vps-4*(DN) (B), *unc-108(nu415)* (C), and *unc-108(nu415);vps-4*(DN) double mutant (D) animals. Bar, 2 μm. (E–H) GLR-1:GFP puncta in the anterior ventral nerve cord of L4 wild-type (E), *unc-108(nu415)* (F), *vps*-4(DN) (G), and *unc-108(nu415);vps-4*(DN) (H) animals were imaged. (I and J) GLR-1::GFP puncta fluorescence (I) and width (J) were quantified for wild-type (n = 38), *unc-108(nu415*) (n = 40), *vps-4*(DN) (n = 34), and *unc-108(nu415); vps-4*(DN) (n = 50) animals. Bar, 10 μm; error bars represent SEM. Values that differ significantly from wild type (by Student's *t* test) are indicated as follows: *$p < 0.01$ and **$p < 0.001$.

of *unc-108* by RNA interference (Lu *et al*., 2008). In *unc-108* mutant interneurons, there is an accumulation of GLR-1::GFP in tubulovesicular structures that colocalize with markers characteristic of early and recycling endosomes, as well as increased abundance of GLR-1::GFP and of GFP::Syntaxin-13 in the ventral nerve cord. Two very recent papers described a defect in the degradation of engulfed cell death corpses in mutants carrying dominant *unc-108* alleles (Lu *et al*., 2008; Mangahas *et al*., 2008). These cell death defects were apparently caused by failure of the phagosomes to mature into lysosomes. A direction function for UNC-108 in endosomal trafficking is also supported by colocalization of UNC-108 with endosomal structures. In coelomocytes, GFP::UNC-108 is localized to early endosomes (Lu *et al*., 2008). In hypodermal cells, UNC-108 was localized to phagosomes containing engulfed cell death corpses (Lu *et al*., 2008; Mangahas *et al*., 2008). Collectively, these results strongly suggest that RAB-2 regulates an aspect of endosomal trafficking in *C. elegans*.

Rab2 belongs to a subfamily of Rabs that includes Rab4 and Rab14. These Rab proteins share a high level of homology within their GTPase domains and hypervariable domains, but they vary near their carboxy-terminal tails. Both Rab4 and Rab14 have been shown to localize to and function at the early endosome (Daro *et al*., 1996; Junutula *et al*., 2004). It has been shown that Rabs sharing a high level of similarity tend to function at similar sites within the cell. For example, Rab7 and Rab9 function at the late endosome (Soldati *et al*., 1995), whereas Rab11 and Rab25 function at the recycling endosome (Ullrich *et al*., 1996; Casanova *et al*., 1999). Based on homology, one might predict that Rab2 could function at endosomes, as we have shown here for UNC-108.

Is UNC-108 Required for COPI-mediated Transport?

Previous studies suggested that Rab2 functions in the COPI-mediated retrograde trafficking of proteins between the Golgi apparatus and the ER, based on overexpression of mutant Rab2 proteins in cell lines (Tisdale and Balch, 1996; Tisdale and Jackson, 1998). Therefore, we analyzed *unc-108* mutants for defects in the COPI pathway. Mutants disrupting retrograde transport secrete KDEL-containing ER resident proteins, e.g., Kar2/BiP (Semenza *et al*., 1990; Andag *et al*., 2001). However, we found that ssVenus::KDEL was retained in the ER, and it was not secreted in *unc-108* mutants. COPI mutants also often have alterations in the morphology of the ERGIC; however, we found that ERGIC morphology (visualized with RFP::BET-1) was unaltered in *unc-108* mutants. In addition to their retrograde transport defects, some COPI mutants also have anterograde transport defects for proteins, e.g., VSV-G. Therefore, we also examined anterograde transport in *unc-108* mutants. Delivery of GLR-1::GFP to the Golgi (assayed as endoglycosidase H resistance), and transport of GFP::UNC-64 Syntaxin out of the ER (assayed by colocalization with ssVenus::KDEL) were both unaffected in *unc-108* mutants. Consequently, it is very unlikely that the GLR-1::GFP trafficking defects observed in *unc-108* mutants are a secondary consequence of a primary defect in COPI-mediated retrograde transport. Our results do not exclude the possibility that UNC-108 also plays a role in retrograde transport in other tissues, or in other systems.

In addition to its well-characterized function in Golgi-to-ER retrograde transport, several articles have documented a requirement for COPI function in endosomal trafficking. In particular, in a mutant Chinese hamster ovary cell line deficient for the epsilon subunit of COPI, defects were observed in the recycling of transferrin receptors, infection by Semliki forest virus and vesicular stomatitis virus viruses, trafficking of internalized horseradish peroxidase to lysosomes, and an absence of multivesicular endosomes (Daro *et al*., 1997; Gu *et al*., 1997). Similar endosomal trafficking defects were also observed in a subset of yeast COPI mutants (Gabriely *et al*., 2007). These defects are likely to reflect direct functions of COPI on endosomes, because a subset of COPI subunits are found on endosomal membranes in both mammalian cells and in yeast (Whitney *et al*., 1995; Gabriely *et al*., 2007). Given these precedents for COPI function in endosomal trafficking, we speculate that UNC-108 (and perhaps Rab2 generally) will play a role in recruiting COPI to endosomal membranes. Consistent with this idea, several yeast COPI mutants have aberrant endosomal structures characteristic of the class E Vps mutants (Gabriely *et al*., 2007), which are similar to the aberrant endosomal structures we describe in *unc-108* mutant interneurons and coelomocytes.

Postendocytic Trafficking of GLR-1

In the ventral cord interneurons, UNC-108/Rab2 was required for the proper distribution of the AMPA-type glutamate receptor GLR-1. Our results suggest that after internalization from the plasma membrane, GLR-1::GFP is sorted into either of two postendocytic pathways. Degradation of GLR-1::GFP is mediated by ubiquitin-mediated sorting into the MVB/lysosome pathway, whereas UNC-108 mediates trafficking of GLR-1::GFP from Syntaxin-13–positive endosomes. Several results support this model. First, in the cell bodies of *unc-108* mutant interneurons, GLR-1::GFP accumulates in tubulovesicular structures that colocalize with endosomal markers. By contrast, GLR-1::GFP accumulates in the limiting membrane of intracellular organelles in *vps-4*(DN) mutants, which are defective for MVB trafficking. Second, the endosomal marker GFP::Syntaxin-13 accumulates in the ventral cord processes of *unc-108* mutants. Third, ubiquitin-mediated degradation of GLR-1::GFP occurs normally in *unc-108* mutants, but was significantly reduced in *vps-4*(DN) mutants. Fourth, the *unc-108(nu415)* and *vps-4*(DN) mutations had additive effects on GLR-1::GFP accumulation. Collectively, these results demonstrate that postendocytic trafficking of GLR-1::GFP is mediated by two parallel pathways, the ubiquitin/MVB pathway and the RAB-2/Syntaxin-13 pathway.

Tubulovesicular endosomes similar to those observed in the cell bodies of *unc-108* mutant interneurons are most commonly associated with recycling endosomes (Prekeris *et al*., 1999). Tubulovesicular recycling endosomes are typically located within neuronal cell bodies, in a perinuclear location (Hopkins *et al*., 1994). These results suggest that UNC-108/Rab2 may function in recycling endosomes. Consistent with this idea, in *unc-108* mutants, GLR-1::GFP accumulates in structures containing the recycling endosome marker Rab8. Thus, we propose that UNC-108/Rab2 regulates sorting of GLR-1::GFP from early or recycling endosomes; however, the target membrane for this pathway remains unclear. Our results do not indicate whether UNC-108/Rab2 promotes recycling of GLR-1 from endosomes to the plasma membrane, or to another intracellular compartment.

Our results are consistent with prior studies of mammalian AMPA receptors. Mammalian AMPA receptors have multiple, alternative postendocytic fates. After internalization, the AMPA receptor GluR1 is sorted into both a recycling pathway, from which it can subsequently be returned to the cell surface, and into a lysosomal degradation pathway (Ehlers, 2000). Similarly, we find that GLR-1 undergoes two postendocytic trafficking pathways, which function in parallel. Very little is known about the cellular mechanisms

that control differential sorting of GluRs between these postendocytic pathways. Different signaling pathways selectively bias GluR1 into either of these two postendocytic pathways. For example, insulin signaling and proteasome activity have both been implicated in postendocytic degradation of GluR1 (Ehlers, 2000; Patrick *et al*., 2003). Our results suggest that Rab2 activity may selectively promote trafficking of GluRs through the recycling endosome pathway.

Implications for Synaptic Plasticity: UNC-108/Rab2 as a Regulator of GluR Recycling

Recycling endosomes are thought to play a pivotal role in activity-dependent remodeling of synapses, e.g., those occurring during LTP. After potentiation, AMPA-type GluRs are inserted into spine membranes, and these newly inserted receptors are thought to be derived from Syntaxin-13–positive recycling endosomes (Lee *et al*., 2001; Park *et al*., 2004). Similarly, potentiated synapses are typically found at larger dendritic spines, and recycling endosomes are proposed to provide the new membrane inserted into potentiated spines (Park *et al*., 2004). Thus, regulation of the recycling endosome pathway is likely to play a role in expressing activity-dependent forms of plasticity. We speculate that the regulation of Rab2 activity may play an important role in this process.

ACKNOWLEDGMENTS

We thank the following for strains, reagents and advice: B. Grant, P. Juo, and *C. elegans* Genetics Stock Center. We also thank members of the Kaplan laboratory for critical comments on this manuscript. This work was supported by grant NS32196 from the National Institutes of Health (to J.M.K.).

REFERENCES

Andag, U., Neumann, T., and Schmitt, H. D. (2001). The coatomer-interacting protein Dsl1p is required for Golgi-to-endoplasmic reticulum retrieval in yeast. J. Biol. Chem. *276*, 39150–39160.

Babst, M., Katzmann, D. J., Snyder, W. B., Wendland, B., and Emr, S. D. (2002). Endosome-associated complex, ESCRT-II, recruits transport machinery for protein sorting at the multivesicular body. Dev. Cell *3*, 283–289.

Bilodeau, P. S., Winistorfer, S. C., Kearney, W. R., Robertson, A. D., and Piper, R. C. (2003). Vps27-Hse1 and ESCRT-I complexes cooperate to increase efficiency of sorting ubiquitinated proteins at the endosome. J. Cell Biol. *163*, 237–243.

Bredt, D. S., and Nicoll, R. A. (2003). AMPA receptor trafficking at excitatory synapses. Neuron *40*, 361–379.

Brenner, S. (1974). The genetics of *Caenorhabditis elegans*. Genetics *77*, 71–94.

Burbea, M., Dreier, L., Dittman, J. S., Grunwald, M. E., and Kaplan, J. M. (2002). Ubiquitin and AP180 regulate the abundance of GLR-1 glutamate receptors at postsynaptic elements in *C. elegans*. Neuron *35*, 107–120.

Carroll, R. C., Beattie, E. C., Xia, H., Luscher, C., Altschuler, Y., Nicoll, R. A., Malenka, R. C., and von Zastrow, M. (1999). Dynamin-dependent endocytosis of ionotropic glutamate receptors. Proc. Natl. Acad. Sci. USA *96*, 14112–14117.

Casanova, J. E., Wang, X., Kumar, R., Bhartur, S. G., Navarre, J., Woodrum, J. E., Altschuler, Y., Ray, G. S., and Goldenring, J. R. (1999). Association of Rab25 and Rab11a with the apical recycling system of polarized Madin-Darby canine kidney cells. Mol. Biol. Cell *10*, 47–61.

Chavrier, P., and Goud, B. (1999). The role of ARF and Rab GTPases in membrane transport. Curr. Opin. Cell Biol. *11*, 466–475.

Colledge, M., Snyder, E. M., Crozier, R. A., Soderling, J. A., Jin, Y., Langeberg, L. K., Lu, H., Bear, M. F., and Scott, J. D. (2003). Ubiquitination regulates PSD-95 degradation and AMPA receptor surface expression. Neuron *40*, 595–607.

Cool, R. H., Schmidt, G., Lenzen, C. U., Prinz, H., Vogt, D., and Wittinghofer, A. (1999). The Ras mutant D119N is both dominant negative and activated. Mol. Cell. Biol. *19*, 6297–6305.

Daro, E., Sheff, D., Gomez, M., Kreis, T., and Mellman, I. (1997). Inhibition of endosome function in CHO cells bearing a temperature-sensitive defect in the coatomer (COPI) component epsilon-COP. J. Cell Biol. *139*, 1747–1759.

Daro, E., van der Sluijs, P., Galli, T., and Mellman, I. (1996). Rab4 and cellubrevin define different early endosome populations on the pathway of transferrin receptor recycling. Proc. Natl. Acad. Sci. USA *93*, 9559–9564.

Donaldson, J. G., Lippincott-Schwartz, J., Bloom, G. S., Kreis, T. E., and Klausner, R. D. (1990). Dissociation of a 110-kD peripheral membrane protein from the Golgi apparatus is an early event in brefeldin A action. J. Cell Biol. *111*, 2295–2306.

Dreier, L., Burbea, M., and Kaplan, J. M. (2005). LIN-23-mediated degradation of beta-catenin regulates the abundance of GLR-1 glutamate receptors in the ventral nerve cord of *C. elegans*. Neuron *46*, 51–64.

Ehlers, M. D. (2000). Reinsertion or degradation of AMPA receptors determined by activity-dependent endocytic sorting. Neuron *28*, 511–525.

Fares, H., and Greenwald, I. (2001). Genetic analysis of endocytosis in *Caenorhabditis elegans*: coelomocyte uptake defective mutants. Genetics *159*, 133–145.

Gabriely, G., Kama, R., and Gerst, J. E. (2007). Involvement of specific COPI subunits in protein sorting from the late endosome to the vacuole in yeast. Mol. Cell. Biol. *27*, 526–540.

Gaynor, E. C., and Emr, S. D. (1997). COPI-independent anterograde transport: cargo-selective ER to Golgi protein transport in yeast COPI mutants. J. Cell Biol. *136*, 789–802.

Grosshans, B. L., Ortiz, D., and Novick, P. (2006). Rabs and their effectors: achieving specificity in membrane traffic. Proc. Natl. Acad. Sci. USA *103*, 11821–11827.

Grunwald, M. E., and Kaplan, J. M. (2003). Mutations in the ligand-binding and pore domains control exit of glutamate receptors from the endoplasmic reticulum in *C. elegans*. Neuropharmacology *45*, 768–776.

Gu, F., Aniento, F., Parton, R. G., and Gruenberg, J. (1997). Functional dissection of COP-I subunits in the biogenesis of multivesicular endosomes. J. Cell Biol. *139*, 1183–1195.

Guo, Q., Vasile, E., and Krieger, M. (1994). Disruptions in Golgi structure and membrane traffic in a conditional lethal mammalian cell mutant are corrected by epsilon-COP. J. Cell Biol. *125*, 1213–1224.

Hart, A. C., Sims, S., and Kaplan, J. M. (1995). Synaptic code for sensory modalities revealed by *C. elegans* GLR-1 glutamate receptor. Nature *378*, 82–85.

Hopkins, C. R., Gibson, A., Shipman, M., Strickland, D. K., and Trowbridge, I. S. (1994). In migrating fibroblasts, recycling receptors are concentrated in narrow tubules in the pericentriolar area, and then routed to the plasma membrane of the leading lamella. J. Cell Biol. *125*, 1265–1274.

Junutula, J. R., De Maziere, A. M., Peden, A. A., Ervin, K. E., Advani, R. J., van Dijk, S. M., Klumperman, J., and Scheller, R. H. (2004). Rab14 is involved in membrane trafficking between the Golgi complex and endosomes. Mol. Biol. Cell *15*, 2218–2229.

Juo, P., and Kaplan, J. M. (2004). The anaphase-promoting complex regulates the abundance of GLR-1 glutamate receptors in the ventral nerve cord of *C. elegans*. Curr. Biol. *14*, 2057–2062.

Juo, P., Harbaugh, T., Garriga G., and Kaplan, J. M. (2007). CDK-5 regulates the abundance of GLR-1 glutamate receptors in the ventral cord of Caenorhabditis elegans. Mol. Biol. Cell *18*, 3883–3893.

Kaiser, C. A., and Schekman, R. (1990). Distinct sets of SEC genes govern transport vesicle formation and fusion early in the secretory pathway. Cell *61*, 723–733.

Katzmann, D. J., Babst, M., and Emr, S. D. (2001). Ubiquitin-dependent sorting into the multivesicular body pathway requires the function of a conserved endosomal protein sorting complex, ESCRT-I. Cell *106*, 145–155.

Lee, S. H., Simonetta, A., and Sheng, M. (2004). Subunit rules governing the sorting of internalized AMPA receptors in hippocampal neurons. Neuron *43*, 221–236.

Lee, S. H., Valtschanoff, J. G., Kharazia, V. N., Weinberg, R., and Sheng, M. (2001). Biochemical and morphological characterization of an intracellular membrane compartment containing AMPA receptors. Neuropharmacology *41*, 680–692.

Lin, J. W., Ju, W., Foster, K., Lee, S. H., Ahmadian, G., Wyszynski, M., Wang, Y. T., and Sheng, M. (2000). Distinct molecular mechanisms and divergent endocytotic pathways of AMPA receptor internalization. Nat. Neurosci. *3*, 1282–1290.

Loria, P. M., Hodgkin, J., and Hobert, O. (2004). A conserved postsynaptic transmembrane protein affecting neuromuscular signaling in *Caenorhabditis elegans*. J. Neurosci. *24*, 2191–2201.

Lu, Q., Zhang, Y., Hu, T., Guo, P., Li, W., and Wang, X. (2008). *C. elegans* Rab GTPase 2 is required for the degradation of apoptotic cells. Development *135*, 1069–1080.

Malinow, R., and Malenka, R. C. (2002). AMPA receptor trafficking and synaptic plasticity. Annu. Rev. Neurosci. *25*, 103–126.

Man, H. Y., Lin, J. W., Ju, W. H., Ahmadian, G., Liu, L., Becker, L. E., Sheng, M., and Wang, Y. T. (2000). Regulation of AMPA receptor-mediated synaptic transmission by clathrin-dependent receptor internalization. Neuron *25*, 649–662.

Mangahas, P. M., Yu, X., Miller, K. G., and Zhou, Z. (2008). The small GTPase Rab2 functions in the removal of apoptotic cells in *Caenorhabditis elegans*. J. Cell Biol. *180*, 357–373.

Maricq, A. V., Peckol, E., Driscoll, M., and Bargmann, C. I. (1995). Mechanosensory signalling in *C. elegans* mediated by the GLR-1 glutamate receptor. Nature *378*, 78–81.

Miller, K. G., Alfonso, A., Nguyen, M., Crowell, J. A., Johnson, C. D., and Rand, J. B. (1996). A genetic selection for *Caenorhabditis elegans* synaptic transmission mutants. Proc. Natl. Acad. Sci. USA *93*, 12593–12598.

Paduch, M., Jelen, F., and Otlewski, J. (2001). Structure of small G proteins and their regulators. Acta Biochim. Pol. *48*, 829–850.

Park, E. C., and Horvitz, H. R. (1986). Mutations with dominant effects on the behavior and morphology of the nematode *Caenorhabditis elegans*. Genetics *113*, 821–852.

Park, M., Penick, E. C., Edwards, J. G., Kauer, J. A., and Ehlers, M. D. (2004). Recycling endosomes supply AMPA receptors for LTP. Science *305*, 1972–1975.

Patrick, G. N., Bingol, B., Weld, H. A., and Schuman, E. M. (2003). Ubiquitin-mediated proteasome activity is required for agonist-induced endocytosis of GluRs. Curr. Biol. *13*, 2073–2081.

Pfeffer, S. R. (2005). Structural clues to Rab GTPase functional diversity. J. Biol. Chem. *280*, 15485–15488.

Pidoux, A. L., and Armstrong, J. (1992). Analysis of the BiP gene and identification of an ER retention signal in *Schizosaccharomyces pombe*. EMBO J. *11*, 1583–1591.

Prekeris, R., Foletti, D. L., and Scheller, R. H. (1999). Dynamics of tubulovesicular recycling endosomes in hippocampal neurons. J. Neurosci. *19*, 10324–10337.

Rak, A., Pylypenko, O., Durek, T., Watzke, A., Kushnir, S., Brunsveld, L., Waldmann, H., Goody, R. S., and Alexandrov, K. (2003). Structure of Rab GDP-dissociation inhibitor in complex with prenylated YPT1 GTPase. Science *302*, 646–650.

Rongo, C., and Kaplan, J. M. (1999). CaMKII regulates the density of central glutamatergic synapses in vivo. Nature *402*, 195–199.

Rongo, C., Whitfield, C. W., Rodal, A., Kim, S. K., and Kaplan, J. M. (1998). LIN-10 is a shared component of the polarized protein localization pathways in neurons and epithelia. Cell *94*, 751–759.

Schaefer, H., and Rongo, C. (2006). KEL-8 is a substrate receptor for CUL3-dependent ubiquitin ligase that regulates synaptic glutamate receptor turnover. Mol. Biol. Cell *17*, 1250–1260.

Semenza, J. C., Hardwick, K. G., Dean, N., and Pelham, H. R. (1990). ERD2, a yeast gene required for the receptor-mediated retrieval of luminal ER proteins from the secretory pathway. Cell *61*, 1349–1357.

Sieburth, D. *et al*. (2005). Systematic analysis of genes required for synapse structure and function. Nature *436*, 510–517.

Sieburth, D., Madison, J. M., and Kaplan, J. M. (2007). PKC-1 regulates secretion of neuropeptides. Nat. Neurosci. *10*, 49–57.

Simmer, F., Moorman, C., van der Linden, A. M., Kuijk, E., van den Berghe, P. V., Kamath, R. S., Fraser, A. G., Ahringer, J., and Plasterk, R. H. (2003). Genome-wide RNAi of *C. elegans* using the hypersensitive rrf-3 strain reveals novel gene functions. PLoS Biol. *1*, E12.

Soldati, T., Rancano, C., Geissler, H., and Pfeffer, S. R. (1995). Rab7 and Rab9 are recruited onto late endosomes by biochemically distinguishable processes. J. Biol. Chem. *270*, 25541–25548.

Song, I., and Huganir, R. L. (2002). Regulation of AMPA receptors during synaptic plasticity. Trends Neurosci. *25*, 578–588.

Speese, S., Petrie, M., Schuske, K., Ailion, M., Ann, K., Iwasaki, K., Jorgensen, E. M., and Martin, T. F. (2007). UNC-31 (CAPS) is required for dense-core vesicle but not synaptic vesicle exocytosis in *Caenorhabditis elegans*. J. Neurosci. *27*, 6150–6162.

Terasaki, M., Jaffe, L. A., Hunnicutt, G. R., and Hammer, J. A., 3rd. (1996). Structural change of the endoplasmic reticulum during fertilization: evidence for loss of membrane continuity using the green fluorescent protein. Dev. Biol. *179*, 320–328.

Tisdale, E. J., and Balch, W. E. (1996). Rab2 is essential for the maturation of pre-Golgi intermediates. J. Biol. Chem. *271*, 29372–29379.

Tisdale, E. J., and Jackson, M. R. (1998). Rab2 protein enhances coatomer recruitment to pre-Golgi intermediates. J. Biol. Chem. *273*, 17269–17277.

Ullrich, O., Reinsch, S., Urbe, S., Zerial, M., and Parton, R. G. (1996). Rab11 regulates recycling through the pericentriolar recycling endosome. J. Cell Biol. *135*, 913–924.

Volchuk, A., *et al*. (2004). Countercurrent distribution of two distinct SNARE complexes mediating transport within the Golgi stack. Mol. Biol. Cell *15*, 1506–1518.

Walworth, N. C., Brennwald, P., Kabcenell, A. K., Garrett, M., and Novick, P. (1992). Hydrolysis of GTP by Sec4 protein plays an important role in vesicular transport and is stimulated by a GTPase-activating protein in *Saccharomyces cerevisiae*. Mol. Cell. Biol. *12*, 2017–2028.

Whitney, J. A., Gomez, M., Sheff, D., Kreis, T. E., and Mellman, I. (1995). Cytoplasmic coat proteins involved in endosome function. Cell *83*, 703–713.

Wicks, S. R., Yeh, R. T., Gish, W. R., Waterston, R. H., and Plasterk, R. H. (2001). Rapid gene mapping in *Caenorhabditis elegans* using a high density polymorphism map. Nat. Genet. *28*, 160–164.

Yeo, S. C. *et al*. (2003). Vps20p and Vta1p interact with Vps4p and function in multivesicular body sorting and endosomal transport in *Saccharomyces cerevisiae*. J. Cell Sci. *116*, 3957–3970.

Zerial, M., and McBride, H. (2001). Rab proteins as membrane organizers. Nat. Rev. Mol. Cell Biol. *2*, 107–117.

Zhang, Y., Grant, B., and Hirsh, D. (2001). RME-8, a conserved J-domain protein, is required for endocytosis in *Caenorhabditis elegans*. Mol. Biol. Cell *12*, 2011–2021.

Zheng, Y., Brockie, P. J., Mellem, J. E., Madsen, D. M., and Maricq, A. V. (1999). Neuronal control of locomotion in C. elegans is modified by a dominant mutation in the GLR-1 ionotropic glutamate receptor. Neuron *24*, 347–361.